Retrieving ice concentration from SMOS

Peter Mills, Georg Heygster, *Member, IEEE,*

***Abstract*—The SMOS-Ice project explored the potential of retrieving sea ice information from the Soil Moisture and Ocean Salinity satellite, a polar-orbiting, L-band radiometer successfully launched in November 2009. Towards this end, radiance measurements were collected over the Northern Baltic during the Pol-Ice campaign. We test a simple ice concentration retrieval algorithm on this data and compare the results to ARTIST Sea Ice (ASI) maps derived from the Advanced Microwave Scanning Radiometer on EOS (AMSR-E). All operational ice concentration algorithms are based on the same principle which, for the campaign data, reduces to a linear scaling of the radiances, because effectively only one channel was available. Because of biases introduced by the differing footprint sizes of the two radiometers (airborne and satellite), the linear flight path and pilot selection of preferred surface type, Pol-Ice and ASI concentrations were compared using three different levels of averaging. In the first case, the individual measurements from the airborne radiometer were compared to interpolated ASI values, in the second, they were averaged over the pixels in the ASI maps and in the third, they were averaged by binning the ASI values in one percent intervals. Correlations were 0.59, 0.67 and 0.76 respectively. Because of the unique operating principle of SMOS, each ground point will be viewed at multiple effective angles within a short time-span. It is proposed to exploit this extra information by interpolating to a single effective viewing angle.**

***Index Terms*—**

I. Introduction

The Soil Moisture and Ocean Salinity (SMOS) instrument is a new satellite microwave radiometer launched in November 2009. It measures in the L-band range at 1.4 GHz with the capability of rendering all four Stokes parameters. To produce a reasonably small footprint size at such a low frequency while keeping antenna weight down, an array of detectors fold out upon deployment to produce an effective aperture equivalent to the span of the array—i.e. much larger than the individual detectors.

While the chief focus of the instrument, as its name implies, is the ocean surface and dry land, it will still return useful information when it is pointing at the cryosphere—the sea ice and glacial ice pack. Even more so than existing microwave radiometers, SMOS will have the advantage of negligible atmospheric contribution to the signal providing true all-weather performance (since radiation at such low frequencies has too little energy to interact strongly with most non-magnetic and non-conducting materials, especially one as thin as the atmosphere.) As preparation for the SMOS project, the Pol-Ice field campaign was conducted in the Northern Baltic in March 2007. This comprised airborne measurements of sea ice brightness temperature using the EMIRAD L-band radiometer [1] and helicopter measurements of ice thickness using the E-M Bird ice thickness detection instrument [2].

Since brightness temperatures over open water tend to be quite distinct from those over ice, the most obvious retrievable quantity from SMOS data is ice concentration, defined as the fraction of ice relative to the total area. Here we test a simple concentration retrieval algorithm on Pol-Ice campaign data and compare the results with satellite-based retrievals.

P. Mills and G. Heygster are both with the Institute of Environmental Physics, University of Bremen, Otto-Hahn-Allee 1, 28359 Bremen, Germany, e-mail: pmills@iup.physik.uni-bremen.de.

Manuscript received July 21, 2010

II. Retrieving ice concentration

Most ice concentration algorithms are predicated on the dual obervation that: 1. different surface types have different, strongly clustered, radiometric signatures and 2. the final radiometric signature at the instrument head is a linear combination of that of the surface types found in the footprint, with weighting factors taking on the values of the relative concentrations. If we form a vector-space from the measurements in which the signatures of the different surface types are assumed invariant and all but one are linearly independent, then it becomes a straightforward matter to derive the relative ice concentrations [2], [3].

We could express this mathematically as follows:

$$\boldsymbol{T_b} = \boldsymbol{T_{b0}} + \sum_{i=1}^{n} (\boldsymbol{T_{bi}} - \boldsymbol{T_{b0}}) C_i \tag{1}$$

where $\boldsymbol{T_b}$ is the vector of brightness temperatures at the instrument head, $\boldsymbol{T_{bi}}$ are the brightness temperatures of the ith surface type, or tie-point, C_i are the relative concentrations and $\boldsymbol{T_{b0}}$ are the brightness temperatures of the nominal background surface type, i.e., of open water. The NASA team algorithm uses a slight variation on this principle: the radiance measurements are transformed by taking the difference of two channels and dividing by their sum, producing a slightly nonlinear retrieval [4], [5]. The influence of ice temperature is thus mitigated since, all other things being equal, brightness temperature varies roughly linearly with temperature (see Equation (2)) and since sea ice brightness temperatures at different microwave channels are strongly correlated [3].

III. Modelling ice brightness temperature

We will use a simple radiative transfer model to simulate the brightness temperature of sea ice at 1.4 GHz. Sea ice is a complex composite comprised mainly of ice crystals, included brine pockets and air bubbles. Because of the small size of the scatterers relative to the wavelength, volume scattering at L-band can be neglected [6]–[9]. In the case of uniform properties within the ice sheet and plane-parallel geometry, the radiative transfer equation for discontinuous media reduces to

the following, closed-form equation, which will henceforth be referred to as the three-layer (air, ice and water) model:

$$T_b = \frac{(R_{ia}-1)\left\{ \begin{array}{c} \left[R_{wi}\tau^2+(1-R_{wi})\tau-1\right]T_{ice}+ \\ (R_{wi}-1)\tau T_w+(R_{ia}-1)R_{wi}\tau^2 T_{sky} \end{array} \right\}}{(R_{ia}R_{wi}\tau^2-1)}, \tag{2}$$

where T_b is the modelled brightness temperature, R_{ia} and R_{wi} are the reflection coefficients at the ice-air and water-ice interfaces, calculated via the Fresnel equations (see (5) and (6), below), T_{ice} is the temperature of the ice, T_w is the water temperature, T_{sky} is the downwelling brightness temperature from the sky and τ is the transmission coefficient:

$$\tau = \exp\left(-\frac{4\pi\nu h \mathrm{Im} n_{ice}}{c\cos\theta_t}\right) \tag{3}$$

where ν is the frequency, h is ice thickness, n_{ice} is the complex refractive index of the ice, c is the speed of light and θ_t is the angle of the radiation as it is transmitted through the ice, calculated from Snell's law:

$$n_1 \sin\theta_1 = n_2 \sin\theta_2 \tag{4}$$

where n_1 is the refractive index of the first medium, n_2 is the refractive index of the second medium, θ_1 is the angle of the ray in the first medium (relative to a normal drawn with respect to the interface) and θ_2 is the angle of the ray in the second medium. Once we have the two angles, the Fresnel equations follow:

$$R_v = \left|\frac{n_2\cos\theta_1 - n_1\cos\theta_2}{n_2\cos\theta_1 + n_1\cos\theta_2}\right|^2 \tag{5}$$

$$R_h = \left|\frac{n_1\cos\theta_1 - n_2\cos\theta_2}{n_1\cos\theta_1 + n_2\cos\theta_2}\right|^2 \tag{6}$$

where R_v and R_h are the reflection coefficients at vertical and horizontal polarization, respectively.

Model results summarizing the approximate behaviour of the signal as the temperature, salinity and thickness are varied can be seen in Figure 1. The figure shows brightness temperatures computed for ice thicknesses ranging from 0 to 2 meters, correcting for the fact that a standard three layer model does not converge to the open water case [10]. The salinity is modelled as an exponential function of ice thickness [11]–[14] for parent waters with two different salinities: the world oceans and for the Baltic sea. Salinity and temperature determine the complex permittivity through the mixture models of Vant et al. [7]. The results suggest that it may be possible to retrieve ice thickness simultaneously with ice concentration only at temperatures close to melting.

For a more complete description of the model, see [2].

IV. Data

The Pol-Ice campaign was conducted in March 2007 in the Northern Baltic and comprised fully polarimetric measurements from an aircraft-mounted, L-band radiometer as well as ice-thickness measurements [2] which will not be used in this study. It is the only reliable source of L-band measurements over sea ice to date. The radiometer used was the EMIRAD which has an angular field-of-view (full-width, half-maximum)

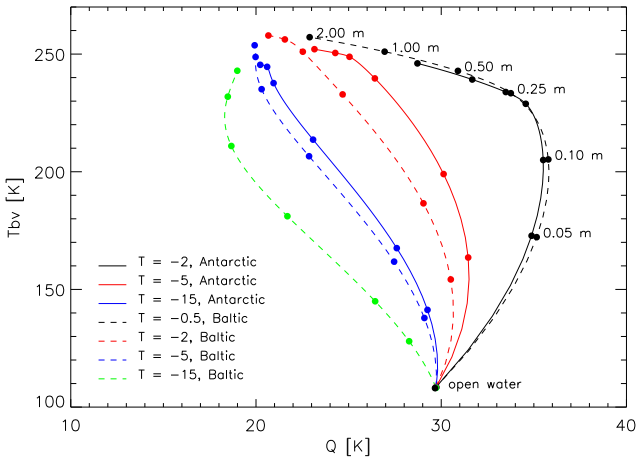

Fig. 1. Model curves for ice at different temperatures in the Baltic (S=5) and in the ocean (S=35). Thickness is varied between 0 and 2 m and marked at intervals by solid dots. Salinity varies as an exponential function of ice thickness. X-axis is the polarization difference or second Stokes component, $Q = T_{bv} - T_{bh}$.

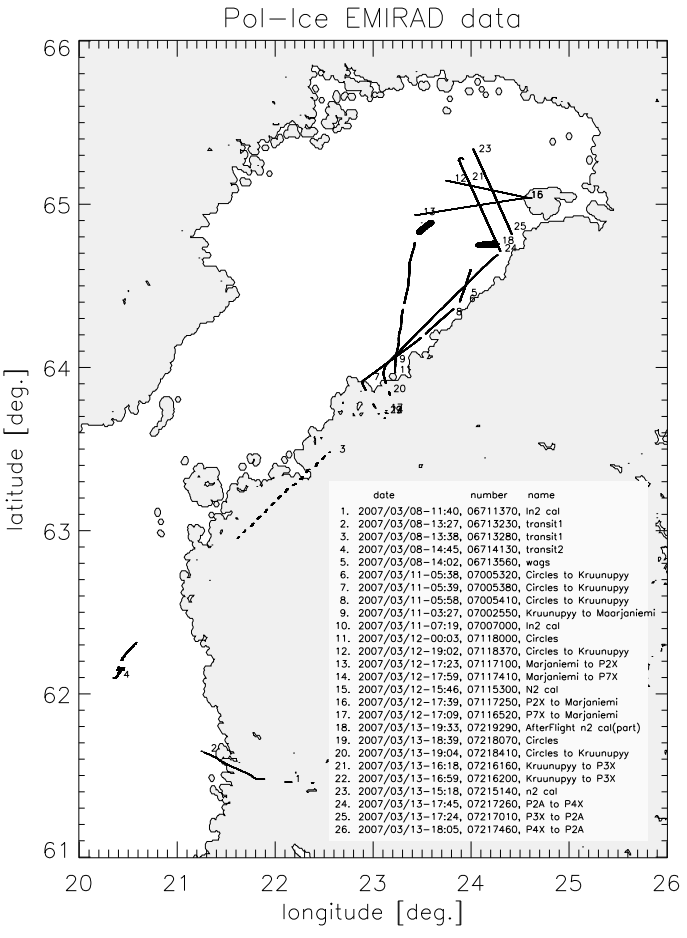

Fig. 2. Map of all Pol-Ice EMIRAD measurements. Flights are labelled by date, name and number.

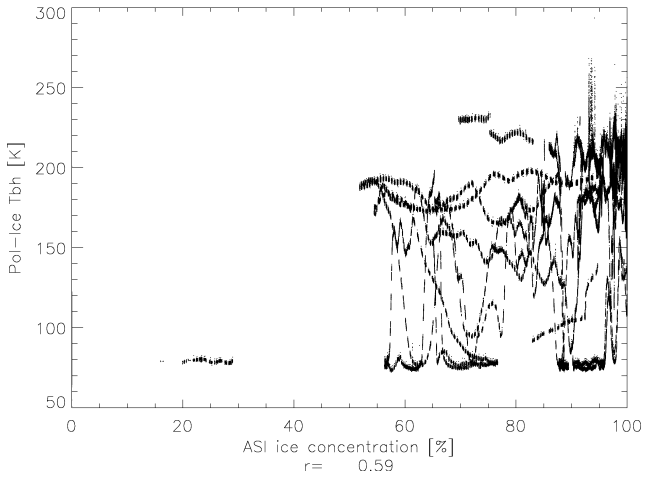

Fig. 3. Measured L-band brightness temperatures from the Pol-Ice field campaign compared to ice concentrations interpolated from ASI ice maps.

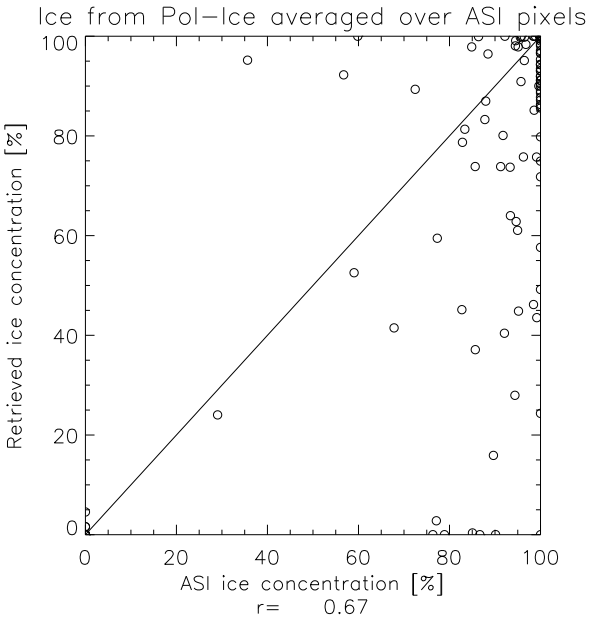

Fig. 4. Ice concentration retrieved from Pol-Ice EMIRAD measurements compared with ASI ice maps. Retrieved concentrations are first averaged over each pixel of the map.

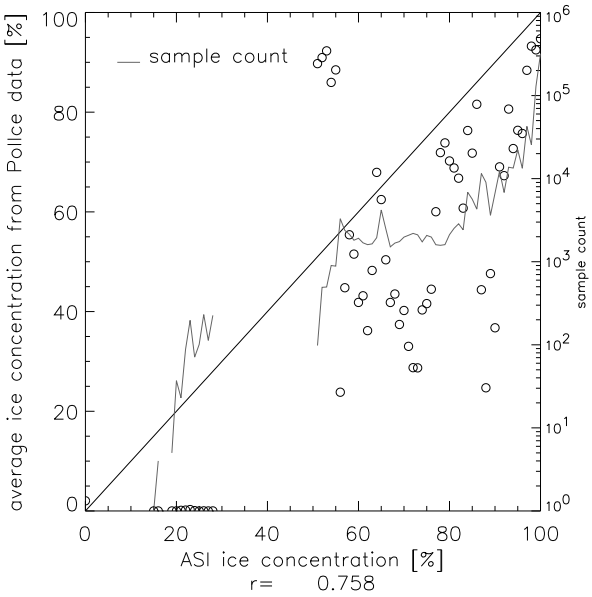

Fig. 5. Ice concentration retrieved from Pol-Ice EMIRAD measurements compared with ASI ice maps. Retrieved concentrations are binned in one percent invervals based on the ASI values and averaged.

of 13.16 degrees [1]. Since the aircraft was flying between 500 m and 600 m, this translates to a footprint size on the order of 250 m. Figure 2 shows most of the radiometer flights labelled by date and time, flight number and flight name.

Ice concentrations for comparison with those derived from the field data are derived from the ASI (ARTIST Sea Ice) algorithm which uses the 89 GHz channel of the Advanced Microwave Scanning Radiometer on EOS (AMSR-E) to derive ice concentrations [15]. These are averaged once a day to maps rectangularly-gridded on a polar-stereographic projection centered at 70 degrees latitutde. The 89 GHz channel is used because it is the highest frequency, therefore it has the best resolution with the final averaging resulting in a mean grid-cell size of 6.25 by 6.25 km. The full record of SSM/I and AMSR-E derived sea ice maps is available online: http://www.iup.uni-bremen.de/iuppage/satellite_index.html

V. Results

It was found that the vertical polarization of the aft-looking radiometer was mal-functioning. Since the third and fourth Stokes components are generated by correlating the h and v components, this makes these two channels suspect also. Thus, there is only one channel to work with and the concentration retrieval in (1) reduces to a linear rescaling of a single brightness temperature. Figure 3 compares ice concentration interpolated from ASI ice maps with EMIRAD brightness temperatures from the Pol-Ice campaign. The correlation, at 0.59, is relatively low, however the radically different footprint sizes—over 3 km for AMSR-E, while for EMIRAD it will be less than 300m—make direct comparison difficult. In particular, the small footprint of the EMIRAD instrument means that pure signals will be more common, thus ice concentration becomes more of an on-off value—either there is ice or there is water. This can be clearly seen in Figure 3 and allows us to easily pick out the two tie-points.

The ice concentrations algorithm will use tie-points of 80 K and 200 K for open water and ice, respectively. Values lower than 80K and higher than 200K are set to 0% and 100% ice concentration, respectively.

The justification for these two tie points is further reinforced by the model results in Figure 1. The model results suggest that sea ice brightness temperatures converge to roughly the same value independent of either the temperature or salinity of the parent water. The values are also close to those chosen for the retrieval, however the retrieval uses more moderate values for the tie points because of the variability in the signatures of pure ice types around the mean. We want to push concentrations

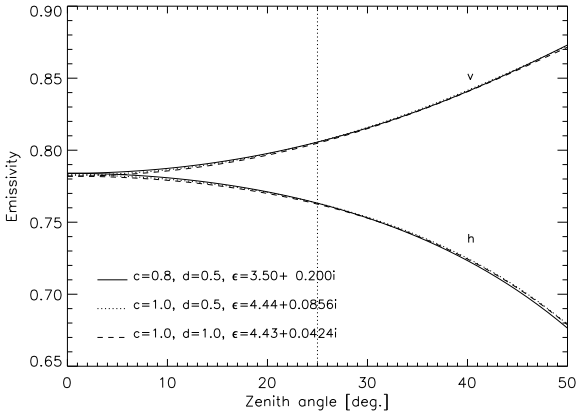

Fig. 6. Viewing angle dependence of sea-ice emissivity simulated using three-layer RT model for three different scenarios of ice thickness, complex permittivity and concentration.

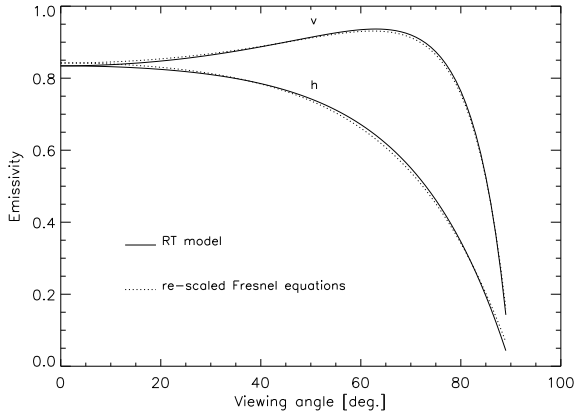

Fig. 7. Viewing angle dependence of sea-ice emissivity simulated using three-layer RT model and of fitted, re-scaled Fresnel equations. For RT model, complex permittivity is $\epsilon = 3.5 + 0.05i$ and ice thickness is h=0.5m. Fresnel equations are for a real refractive index of $n = 1.91$ and have been rescaled using $e'_p = ae_p + b$ where e_p is emissivity at polarization p and $a = 0.901$ and $b = 0.050$ are constants.

close to the pure types over the border to a pure type if the radiance signature is within this variability.

To address the issue of different footprint sizes, we average all the EMIRAD measurements within each pixel of the ice map and compare ice concentrations pixel-by-pixel. The ASI ice maps are averaged daily to bins that are regularly-gridded, along a polar-stereographic projection. This averaging does not significantly reduce the resolution of the instrument and is done mainly to take advantage of the many overlapping swaths at high latitudes. EMIRAD measurements from Pol-Ice are similarly averaged by first converting measurement locations to the projection coordinates and then searching for the matching ASI grid point. Results are shown in Figure 4.

Even though we have matched the instrument resolution to the lower of the two, results may still be biased because the pilot may be deliberately searching out either ice-covered or open water surface and because the linear flight path traces out only a narrow line of measurements across the broad satellite footprint. To address this, we further average the results by collecting them in one percent bins based on ASI ice concentration. This generates the graph seen in Figure 5 which shows a much improved correlation.

VI. Discussion

The unique operating principle of the SMOS instrument means that each point on the ground will be viewed from multiple angles by overlapping measurements —each measurement from the instrument will consist of a single large footprint comprising multiple pixels of varying size and effective viewing angle [16]. With a high sampling rate, these footprints will overlap. Can extra information be gained by having measurements from different viewing angles? Results from the model described in Section III suggest that the best use of these extra measurements is to interpolate them to a single effective viewing angle.

Figure 6 shows modelled sea ice emissivity as a function of viewing angle for three scenarios of varying ice concentration, thickness and complex permittivity. These scenarios are designed to be degenerate at an angle of 25 degrees. Although we would expect them to diverge at other viewing angles, they are almost identical, certainly to within the instrument noise. It was found that the viewing angle dependence of ice emissivity models of the type described in Equation (2) can be well approximated by Fresnel equations that have been linearly re-scaled:

$$e'_p = ae_p + b \tag{7}$$

where e'_p is the fitted emissivity at polarization p (h or v) and $e_p = 1 - R_p$ is the emissivity as calculated from the Fresnel equations (5) and (6). Figure 7 demonstrates the procedure which works as well if brightness temperature is modelled with more than one ice layer.

VII. Conclusion

Ice concentrations derived from Pol-Ice campaign data were compared with ASI satellite- based retrievals. Correlations were between 0.59 and 0.76 depending on the level of averaging empoyed. Several influences make the averaging procedures necessary: the two instruments (satellite and airborne) have very different footprint sizes as well as different temporal resolutions; the airborne radiometer had a linear path, during which the pilot may have been searching out specific surface types. Another possible error source: the ASI algorithm is designed for the high salinity of the open ocean rather than the brackish waters of the Baltic Sea.

This comparison exercise was conducted as part of the SMOSIce project, which aims to prepare retrieval algorithms for data collected over sea ice by the Soil Moisture and Ocean Salinity (SMOS) satellite which was successfully launched in November 2009. The SMOS instrument will sample the same stretch of ground at multiple effective viewing angles within a short time span. Ice emissivity models suggest that this data will provide little extra information. An effective use of it, however, would be to interpolate to a single effective viewing angle, thus helping to stabilize the measurements.

ACKNOWLEDGMENT

The authors would like to thank the following people involved in the SMOS-Ice project for valuable discussions: Catherine Bouzinac, Mark Drinkwater. Matthias Drusch, Stefan Hendricks, Lars Kaleschke, Christian Maetzler and Rasmus Tonboe. This work was supported by ESA contract 21130/08/NL/EL, *L-Band Radiometry for Sea Ice Applications*.

REFERENCES

[1] N. Skou, S. S. Sobjaerg, and J. Balling, "EMIRAD-2 and its use in the CoSMOS Campaigns," Electromagnetic Systems Section, Danish National Space Center, Technical University of Denmark, Tech. Rep. ESTEC Contract No. 18924/05/NL/FF, 2007.

[2] G. Heygster, S. Hendricks, L. Kaleschke, N. Maass, P. Mills, D. Stammer, R. T. Tonboe, and C. Haas, "L-Band Radiometry for Sea-Ice Applications," Institute of Environmental Physics, University of Bremen, Tech. Rep. final report for ESA/ESTEC Contract N. 21130/08/NL/EL, 2009.

[3] D. A. Rothrock, D. R. Thomas, and A. S. Thorndike, "Principal Component Analysis of Satellite Passive Microwave Data Over Sea Ice," *Journal of Geophysical Research*, vol. 93, no. C3, pp. 2321–2332, March 1988.

[4] J. C. Comiso, D. J. Cavalieri, C. L. Parkinson, and P. Gloersen, "Passive microwave algorithms for sea ice concentration: A comparison of two techniques," *Remote Sensing of the Environment*, vol. 60, pp. 357–384, 1997.

[5] T. Markus and D. J. Cavalieri, "An Enhancement of the NASA Team Sea Ice Algorithm," *IEEE Transactions on Geoscience and Remote Sensing*, vol. 38, no. 3, pp. 1387–1398, May 2000.

[6] D. G. Barber, A. K. Fung, T. C. Grenfell, S. V. Nghiem, R. G. Onstott, V. I. Lytle, D. K. Perovich, and A. J. Gow, "The role of snow on microwave emission and sacttering over first-year sea ice," *IEEE Transactions on Geoscience and Remote Sensing*, vol. 36, no. 5, pp. 1750–1763, September 1998.

[7] M. R. Vant, R. O. Ramseier, and V. Makios, "The complex-dielectric constant of sea ice at frequencies in the range 0.1-40 GHz," *Journal of Applied Physics*, vol. 49, no. 3, pp. 1264–1280, March 1978.

[8] A. Stogryn, "A study of microwave brightness temperatures of snow from the point of view of strong fluctuation theory," *IEEE Transactions on Geoscience and Remote Sensing*, vol. GE-24, no. 2, pp. 220–231, March 1986.

[9] K.-P. Johnsen, "Radiometrische Messungen im arktischen Ozean–Vergleich von Theorie und Experiment," Ph.D. dissertation, Universitaet Bremen, Otto-Hahn Allee 1, Bremen, Germany, 1998.

[10] J. D. Menashi, K. M. St. Germain, C. T. Swift, J. C. Comiso, and A. W. Lohanick, "Low-frequency passive-microwave observations of sea ice in the weddell sea," *Journal of Geophysical Research*, vol. 98, no. C12, pp. 22 569–22 577, December 1993.

[11] W. F. Weeks and S. F. Ackley, *The Geophysics of Sea Ice*, ser. NATO ASI Series B: Physics. Plenum Press, 1985, vol. 146, ch. 2.

[12] G. Cox and W. Weeks, "Numerical simulations of the profile properties of undeformed first-year sea ice during the growth season," *Journal of Geophysical Research*, vol. 93, no. C10, pp. 12 499–12 460, October 1988.

[13] W. B. Tucker, D. K. Perovich, A. J. Gow, W. F. Weeks, and M. R. Drinkwater, "Physical Properties of Sea Ice Relevant to Remote Sensing," in *Microwave Remote Sensing of Sea Ice*, ser. Geophysical Monographs. American Geophysical Union, 1992, no. 68, ch. 2, pp. 9–28.

[14] J. K. Ehn, B. J. Hwang, R. Galley, and D. G. Barber, "Investigations of newly formed sea ice in the Cape Bathurst polynya: 1. Structural, physical and optical properties," *Journal of Geophysical Research*, vol. 112, no. C05002, 2007, doi=10.1029/2006JC003702.

[15] G. Spreen, L. Kaleschke, and G. Heygster, "Sea ice remote sensing using AMSR-E 89 GHz channels," *Journal of Geophysical Research*, vol. 113, no. C02S03, 2008, doi=10.1029/2005JC003384.

[16] Y. H. Kerr, "Soil Moisture and Ocean Salinity: Radiometry applied to soil Moisture and Salinity Measurements," CESBIO, Toulouse, Tech. Rep., November 1998, the Living Planet Programme Earth Explorer Missions.

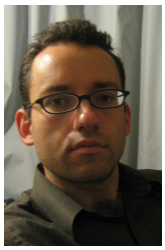

Peter Mills was born on December 22, 1973 in Montreal, Canada. He received a Bachelor's Degree in Physics from the University of Waterloo in Ontario, Canada and a Master's Degree in Environmental Physics from the University of Bremen, Germany. Peter has worked most of his adult life in the fields of climate and remote-sensing research, including some of the most hotly discussed areas such El Ninio/Southern Oscillation and ozone detection. He has a passion for all forms of rational inquiry, particularly those that cross disciplines. Examples include chaos theory, artificial life, complexity theory and cognitive science. He has authored two papers on chaos theory.

Georg Heygster Georg Heygster (M'00) received the Diploma degree in solid-state physics and the Ph.D. degree in digital image processing from the University of Goettingen, Goettingen, Germany, in 1976 and 1979, respectively.

He served as a Consultant with the Computer Center of the University of Bremen, Bremen, Germany, from 1979 to 1988. Since then, after working for a year on the imaging mechanisms of scanning acoustic microscopes, he has been Head of the Geophysical Analysis of Satellite Images group at the Institute of Environmental Physics, University of Bremen. His research activities include passive and active microwave remote sensing, particularly of both surface and atmospheric parameters in the high latitudes, various aspects of the hydrological cycle, long-term trends, and retrieval techniques. He was or still is Principal Investigator or Coinvestigator of many research projects funded by the European Union, the European Space Agency, the German Research Council, and the Japan Aerospace Exploration Agency. These projects include the development of sensor soft- and hardware, conducting campaigns, the final data analysis from multi- and single-sensor data to geophysical parameters, and the interpretation and application of these results in many areas such as meteorology, climatology, and oceanography.